Article | Received 3 June 2024; Revised 17 August 2024; Accepted 25 August 2025; Published 1 September 2025
https://doi.org/10.55092/bm20250012

A highly bioactive yak collagen mesotherapy for rejuvenation of photoaging skin

Shimeng Xu[1,2,†], Yi Yang[1,2,†], Jingting Zhang[1,2], Guangyu Liu[1,2], Xiuxia Sun[2,3,*] and Jianxi Xiao[1,2,*]

[1] State Key Laboratory of Nature Product Chemistry, College of Chemistry and Chemical Engineering, Lanzhou University, Lanzhou 730000, China
[2] Gansu Engineering Research Center of Medical Collagen, Lanzhou 730000, China
[3] School of Pharmacy, Lanzhou University, Lanzhou 730000, China

† These authors contributed equally to this work.

* Correspondence authors; E-mails: sunxx@lzu.edu.cn (X.S.); xiaojx@lzu.edu.cn (J.X.).

Highlights:

- Introduced the first yak Col-M as a multifunctional treatment for photoaged skin.
- Demonstrated antioxidant, whitening, moisturizing, and regenerative effects with validated efficacy in cellular and animal models.
- Achieved collagen regeneration, dermal density enhancement, and skin barrier restoration with excellent biosafety and translational potential.

Abstract: Ultraviolet (UV) radiation was one of the primary contributors to skin aging. Prolonged exposure to UV rays accelerated the degradation of collagen, resulting in various photoaging-related skin problems, including wrinkles, dryness, and hyperpigmentation. Mesotherapy was a widely utilized skin repair method in the field of aesthetic medicine; however, it faced challenges such as biosafety concerns and monofunctionality. Herein, we developed for the first time a highly bioactive yak collagen mesotherapy (Col-M) for the rejuvenation of photoaging skin. Through experiments measuring DPPH and ABTS radical scavenging rates, tyrosinase inhibition rates, and zebrafish efficacy evaluation experiments, the multifunctional Col-M was identified. This mesotherapy demonstrated exceptional antioxidant, whitening, moisturizing, repair-promoting, and soothing effects. Animal studies demonstrated that the Col-M increased dermal density, improved skin tone, enhanced skin hydration, and restored transcutaneous water loss (TEWL). The Col-M stimulated fibroblasts, providing an optimal physiological environment that promoted collagen regeneration and improved photoaged skin. H&E staining revealed that Col-M effectively avoided triggering an inflammatory response while demonstrating the ability to suppress epidermal hyperplasia. Masson trichrome staining illustrated that the Col-M promoted collagen regeneration and expedited the remodeling process of photoaged skin. In photoaged mice skin, Col-M elevated hydroxyproline content, superoxide dismutase (SOD) activity, and glutathione reductase (GSH) levels, concurrently reducing malondialdehyde (MDA) levels. The Col-M

provided an effective treatment for photoaged skin, presenting significant application potential in the fields of dermatology and regenerative medicine.

Keywords: yak collagen; collagen mesotherapy; photoaging skin rejuvenation; antioxidant activity; collagen regeneration; skin repair

1. Introduction

Skin aging is classified into endogenous aging driven by time and exogenous aging caused by environmental factors [1–3]. Photoaging caused by prolonged UV exposure is the primary contributor to exogenous aging and its main clinical manifestations include wrinkles, rough texture, and pigmentation [4–7]. The structural integrity of the skin relies heavily on collagen, a protein abundantly found in the dermal matrix that significantly degrades in photoaged skin [8–10]. Therefore, the establishment of effective interventions to improve skin photoaging is of utmost importance.

Mesotherapy is a minimally invasive technique that delivers active ingredients into the dermis to stimulate collagen production, enhance hydration, and improve microcirculation. With its advantages of minimal trauma, low side effects, and quick recovery, it has become widely used in aesthetic medicine [11–13]. Recent clinical and preclinical studies have demonstrated its effectiveness in improving skin quality, including split-face randomized controlled trials of non-crosslinked hyaluronic acid showing enhanced hydration, elasticity, and reduction of fine wrinkles [14,15]. Among various agents, hyaluronic acid-based mesotherapy is widely used due to its well-established safety profile and ability to promote collagen regeneration and improve skin turgor. However, the lack of cross-linking renders it susceptible to rapid degradation by endogenous hyaluronidase, resulting in limited durability and reduced efficacy [16–18]. To overcome these limitations, collagen-based mesotherapy has been explored as an alternative, as collagen can directly promote extracellular matrix synthesis and help mitigate the degradation of collagen and elastic fibers in photoaged skin [19,20]. Nevertheless, current recombinant collagen formulations are often costly and offer relatively singular efficacy, which restricts their broader clinical adoption.

Collagen is a widely utilized biomedical material where safety and efficacy are critical factors for its medical applications [21–23]. Yaks typically inhabit high-altitude snow mountain environments and remain isolated from modern industrial farming systems, significantly reducing their risk of exposure to mad cow disease contamination [24,25]. Compared to local cattle, yaks have a growth cycle of up to six years that results in higher protein content with a comprehensive amino acid profile, lower fat content, and abundant collagen making them an exceptional source of collagen [26]. Furthermore, yak collagen is free from heavy metal contamination, drug residues and other pollutants to ensure its purity [27]. Moreover, yak collagen's adaptation to high-altitude environments endows it with unique molecular characteristics, such as higher proline and hydroxyproline content and enhanced triple-helix stability, which may contribute to its superior bioactivity and lower immunogenicity. Therefore, yaks represent an unparalleled source of premium collagen characterized by its natural, eco-friendly, high-quality, and safe properties that make it an ideal raw material.

We have for the first time reported a multifunctional yak collagen mesotherapy for skin rejuvenation of photoaging model mice (Scheme 1). The free radical scavenging and tyrosinase inhibition assays indicated that the Col-M possesses superior antioxidant properties and whitening effects. The results of the

circular dichroism (CD) spectra indicated that the yak collagen in Col-M retains its complete triple-helix structure. The rabbit pyrogen and hemolysis tests demonstrated that the Col-M exhibits excellent biosafety, with no pyrogenic response or hemolytic risk. After injection into photoaging mice skin, the Col-M increased dermal density, enhances skin brightness, boosted hydration levels, reduced moisture loss, and promoted collagen regeneration. The Col-M shows promising application prospects in the field of medical aesthetics, facilitating advancements in skin rejuvenation.

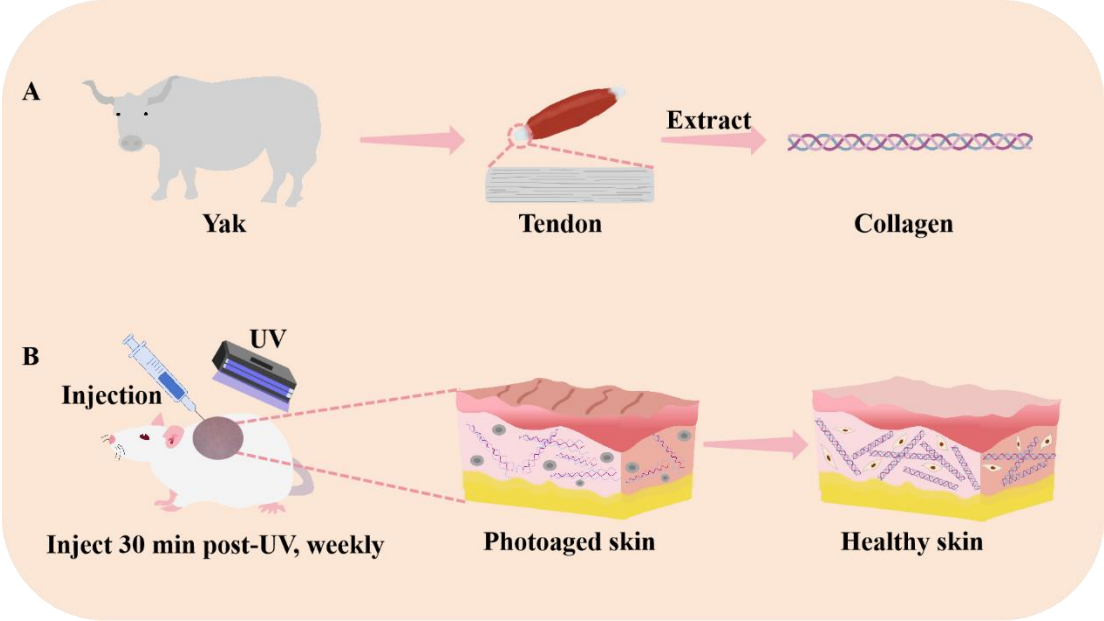

Scheme 1. Schematic diagram of a highly bioactive yak collagen mesotherapy for rejuvenation of photoaging skin.

2. Methods

2.1. Radical scavenging and tyrosinase inhibition assay

In a 96-well plate, 100 μL of a 0.10 mg/mL DPPH ethanol solution was combined with 100 μL of test solutions at various concentrations. The resulting mixture was incubated in the dark at room temperature for 30 minutes. Absorbance was subsequently measured at 517 nm using a Tecan Infinite F200/M200 multifunction microplate reader [28]. The DPPH radical scavenging activity was then determined using the following formula:

$$\text{DPPH radical scavenging rate (\%)} = \left(1 - \frac{D_t - D_b}{D_c}\right) \times 100\%$$

D_t represents the absorbance of the experimental group (sample solution + DPPH radical solution). D_b represents the absorbance of the blank control group (sample solution + anhydrous ethanol). D_c represents the absorbance of the control group (water + DPPH radical solution).

The ABTS working solution was prepared by mixing 7 mM ABTS solution and 2.45 mM potassium persulphate in equal volume. The reaction mixture was maintained at room temperature in the dark for 12–16 hours. The ABTS working solution was then diluted with deionized water to obtain the absorbance of 0.70 ± 0.02 at 734 nm. 20 μL of different concentration of sample solution was added to 180 μL diluted ABTS working solution. The reaction mixture was kept in the dark at room temperature

for 5 min. The absorbance was then measured at 734 nm. The formula for calculating the ABTS radical scavenging rate was as follows:

$$\text{ABTS radical scavenging rate (\%)} = \left(1 - \frac{A_t - A_b}{A_c}\right) \times 100\%$$

A_t represents the absorbance of the experimental group (sample solution + ABTS solution). A_b represents the absorbance of the blank control (sample solution + water). A_c represents the absorbance of the control group (water solution + ABTS solution).

In a 96-well plate, the required buffer solution (0.2 mol/L PBS at pH 6.8), sample solution, and L-tyrosine solution should be added sequentially. The mixture was then incubated in a water bath maintained at 37 ℃ for 10 minutes. Following this incubation, the corresponding tyrosinase solution (0.05 mg/mL) was added, and the reaction was sustained at 37 ℃ for an additional 10 minutes. Finally, the absorbance of each solution was measured at 475 nm. The calculation for the inhibitory rate of the samples against tyrosinase was as follows:

$$\text{Tyrosinase inhibition rate (\%)} = \left(1 - \frac{T_2 - T_1}{C_2 - C_1}\right) \times 100\%$$

C_1 represents the absorbance measured in the absence of both the sample and enzyme solutions. C_2 represents the absorbance measured with only the enzyme solution present. T_1 represents the absorbance measured with only the sample solution present. T_2 represents the absorbance measured in the presence of both the sample and enzyme solutions.

2.2. Zebrafish experiments

Zebrafish share key genetic and structural similarities with mammalian skin, including layered epidermis and dermis, collagen-rich stroma, and conserved wound-healing mechanisms [29,30]. Their transparent embryos, rapid regeneration, and high fecundity allow real-time observation and high-throughput screening of anti-photoaging compounds [31]. These features make zebrafish a validated and practical model for studying skin photoaging and rejuvenation.

2.2.1. Zebrafish hydration and moisturization test

Wild-type AB zebrafish at 3 days post-fertilization (dpf) were used to perform the experiments. 70 zebrafish at 3 dpf were randomly assigned to seven groups: the normal group, model group, and 5 sample treatment groups (Col, HA + Col, DG + Col, DTd + Col, and Ceramide + Col). The normal group was incubated with fish embryo culture medium. The model group was incubated with a 1.5% sodium chloride solution. The 5 treatment groups were incubated with a mixture solution containing 1.5% sodium chloride, 0.1 mg/mL collagen, and 0.5 mg/mL moisturizer. Zebrafish embryos were placed in a 96-well cell culture plate, with one embryo per well, and 200 μL of the appropriate solution was added to each well. The embryos were incubated in a temperature-controlled incubator at 28 ± 1 ℃ for 15 minutes. After incubation, the zebrafish were laid flat on glass slides, photographed with a stereomicroscope, and their tail area and length were analyzed using ImageJ software. The average tail area and length for each group were calculated using the following formula:

$$\text{Relative tail length (\%)} = \frac{A}{B} \times 100\%$$

$$\text{Relative area of caudal fin (\%)} = \frac{C}{D} \times 100\%$$

A: the length after dehydration. B: the length before dehydration. C: the caudal fin area after dehydration. D: the caudal fin area before dehydration.

2.2.2. Zebrafish tissue repair and regeneration test

Healthy zebrafish embryos at 3 dpf were utilized for the experiments. After anesthetizing the zebrafish larvae with 0.016% tricaine, their tail fins were excised at the distal end of the spine using a scalpel through a stereomicroscope. 80 fish embryos with tail fins removed were randomly divided into 8 groups: Normal, Model, Col (0.1 mg/mL), Cae + Col (0.1 mg/mL + 0.1 mg/mL), Ceramide + Col (0.1 mg/mL + 0.1 mg/mL), BFE + Col (0.1 mg/mL + 0.1 mg/mL), Allantoin + Col (0.1 mg/mL + 0.1 mg/mL), and GHK + Col (0.1 mg/mL + 0.1 mg/mL). The embryos were transferred to a 96-well plate with one embryo per well. The normal and model groups were administered 0.2 mL of fish embryo culture medium, while the sample groups were given 0.2 mL of their respective sample solutions. The embryos were incubated in a temperature-controlled incubator at 28 ± 1 °C for 72 hours, after which they were photographed under a microscope. Tail fin areas were measured using ImageJ software and subsequently analyzed statistically [32].

2.2.3. Zebrafish anti-wrinkle test

Experiments were conducted using wild-type AB zebrafish at 2 dpf. A total of 80 zebrafish were randomly divided into eight groups and distributed across 6-well plates with 10 zebrafish per well in a final volume of 3 mL. These groups included Normal, Model, Col (0.1 mg/mL), β-glucan + Col (0.1 mg/mL + 0.1 mg/mL), NMN + Col (0.1 mg/mL + 0.1 mg/mL), L-Carnosine + Col (0.1 mg/mL + 0.1 mg/mL), PDRN + Col (0.1 mg/mL + 0.1 mg/mL), and GHK + Col (0.1 mg/mL + 0.1 mg/mL). All groups except the Normal group were exposed to ultraviolet radiation. The specific irradiation protocol was as follows: three radiation stages, each lasting 15 minutes at an intensity of 2.0–2.5 mW/cm² with a 30-minute interval between stages. All groups were then incubated in the dark at 28 °C for 22 hours. Ten zebrafish were randomly selected from each group and observed under a microscope. The caudal fin areas were measured using Image J software and then analyzed statistically.

$$\text{Wrinkle resistance rate (\%)} = \frac{\text{S} - \text{M}}{\text{N} - \text{M}} \times 100\%$$

S represents the tail fin area of the irradiated sample group. M refers to the tail fin area of the irradiated model group. N denotes the tail fin area of the normal group.

2.2.4. Zebrafish embryo smoothing test

Healthy zebrafish embryos (70 in total) at 3 dpf were placed in 96-well plates with 2 embryos per well. These zebrafish were divided into seven groups: Normal (treated with a normal culture solution), Model (exposed to 0.5 mg/mL SDS), Col (treated with 0.5 mg/mL SDS and 0.1 mg/mL Col), NMN + Col (treated with 0.5 mg/mL SDS, 0.1 mg/mL NMN, and 0.1 mg/mL Col), PDRN + Col (treated with 0.5 mg/mL SDS, 0.1 mg/mL PDRN and 0.1 mg/mL Col), Allantoin + Col (treated with 0.5 mg/mL SDS, 0.1 mg/mL Allantoin and 0.1 mg/mL Col), Cae + Col (treated with 0.5 mg/mL SDS, 0.1 mg/mL Cae and 0.1 mg/mL Col).

After 15 minutes of treatment, the embryos were observed under a stereomicroscope for one minute. The number of spinning motions of the embryos in each group was recorded.

2.3. Circular dichroism spectra of Col-M

Circular dichroism (CD) spectra were recorded on a JASCO J1500 spectrometer with built-in temperature regulation. Col and Col-M solutions were separately prepared in 20 mM phosphate buffer (pH 7.0) and equilibrated at 4 ℃ for 24 hours before the experiments. The experiments were conducted using a 1 mm path length cell. Spectra were recorded over a wavelength range of 190–260 nm with a step size of 1.0 nm and an averaging time of 1.0 second per point. The thermal denaturation profile was assessed by monitoring CD intensity at 225 nm as the temperature was progressively increased. The process began at 1 ℃/min from 4 ℃ to 20 ℃, followed by 0.3 ℃/min from 20 ℃ to 50 ℃, and concluded at 1 ℃/min from 50 ℃ to 80 ℃, with stabilization intervals of 1 minute at each step. The melting temperature (T_m) was derived from the first derivative of the thermal denaturation curve. Data processing and visualization were carried out using Origin software.

2.4. In vitro cell experiment

The assessment of Col-M's cytotoxicity was evaluated with CCK-8 assays. Human dermal fibroblasts (HDF) were cultured at 37 ℃ in a 5% CO_2 environment using high-glucose MEM medium supplemented with 10% (v/v) fetal bovine serum and 1% (v/v) penicillin-streptomycin. The Col-M at high concentration was diluted in high-glucose MEM to obtain samples with varying concentrations (0%, 20%, 50%, 100%, 200%). The cells were then subjected to treatment with 0.25% (w/w) trypsin before being distributed into 96-well plates, ensuring a cell density of 7×10^3 per well. A suspension of 7000 HDF cells in 100 μL was added to each well of the plate and incubated for 24 hours at 37 ℃. Then varying concentrations of the sample were introduced to the 96-well plates and incubated for another 24 hours. Subsequently, 10 μL of CCK-8 solution was added to each well and incubated for 1 to 3 hours at 37 ℃. The baseline culture medium served as a blank control (n = 6), and the optical density (OD) at 450 nm was recorded using a Tecan Infinite F200/M200 multifunction microplate reader. Cell viability was determined using the specified formula:

$$\text{Cell viability (\%)} = \frac{\text{A} - \text{C}}{\text{B} - \text{C}} \times 100\%$$

A denotes the OD value of the sample. B signifies the OD value of the blank control. C indicates the OD value of the medium.

2.5. Animal experiments

2.5.1. Pyrogen and hemolysis test of Col-M

To assess the *in vivo* pyrogenicity and hemolytic safety of the collagen mesotherapy formulation (Col-M), animal experiments were conducted using six healthy female New Zealand White rabbits (each weighing approximately 2.0 kg), obtained from the Animal Experiment Center of Lanzhou University.

Before the experiment, temperatures were recorded at 30-minute intervals, and the average temperature, with a variation not exceeding 0.2 ℃, was established as the rabbits' normal body

temperature. Following this, 2 mL of 0.9% saline and Col-M were injected into the marginal ear vein separately with temperature readings taken six times for each. The temperature variation was calculated by taking the highest recorded temperature and subtracting the normal temperature from it. A biomaterial was deemed non-thermogenic if the temperature change for each individual rabbit remained within 0.6 ℃, and the total temperature differences for all rabbits in the group were less than 1.3 ℃ [33].

5 mL of an anticoagulant solution were combined with 1 mL of freshly collected rabbit blood, followed by centrifugation to isolate the red blood cells. A 0.2 mL portion of the red blood cell suspension was diluted in 0.9% saline, and the resulting solution was then mixed separately with 0.9% saline, deionized water, and Col-M. The mixtures were incubated at 37 ℃ for 1 hour, followed by a further 3 hours at room temperature. Afterward, the supernatant was obtained through centrifugation, and the OD of hemoglobin was measured at 545 nm. The hemolysis rate (HR, %) was then determined using the following formula [34]:

$$\mathrm{HR}(\%) = \frac{\mathrm{OD_a} - \mathrm{OD_b}}{\mathrm{OD_c} - \mathrm{OD_b}} \times 100\%$$

OD_a: the OD values of the test samples. OD_b: the OD values of the 0.9% saline. OD_c: the OD values of the ultrapure water.

2.5.2. Construction of a photoaging mice model

To establish a murine model for evaluating the anti-photoaging efficacy of the collagen mesotherapy formulation (Col-M), animal experiments were conducted in accordance with the ethical guidelines approved by the Ethics Committee of the College of Chemistry and Chemical Engineering, Lanzhou University (Approval No. G09, 20220711). A total of 90 female Kunming mice, aged 6 to 8 weeks, were purchased from the Lanzhou Animal Experiment Center. Prior to the experiment, the mice had their dorsal fur shaved, and they were placed in specially designed cages that were fitted with protective eye shields. The mice were randomly assigned to five groups, each consisting of 18 mice: The normal group consisted of healthy, untreated mice. The model group consisted of photoaged mice that received no treatment. The Col group was injected with 200 μL of a 0.1 mg/mL collagen solution, while the control group received 200 μL of a commercially available mesotherapy solution. The Col-M group received an injection of 200 μL of yak collagen mesotherapy solution.

The mice were exposed to UV radiation three times per week for eight consecutive weeks, with each exposure lasting 20 minutes. The total UVA and UVB doses were 20.4 J/cm² and 1.44 J/cm², respectively. During the 2nd, 4th, and 8th weeks of the experiment, the mice underwent fur shaving, followed by anesthesia using a 10% sodium pentobarbital solution. Afterward, the mice were euthanized, and skin samples were harvested from the injection sites for further analysis.

2.5.3. Combo assessment of skin condition

The mice's skin appearance was assessed using Combo dermatoscopy, and skin density was measured with Combo ultrasound imaging. Prior to each ultrasound assessment, a thin layer of gel was applied to the probe tip to facilitate proper contact. Key indicators of skin health, such as skin color, hydration levels, and transepidermal water loss (TEWL), were measured. The assessment involved identifying specific measurement locations on the dorsal skin, with three readings taken at each site to ensure accuracy.

2.5.4. Histological assessment

To evaluate inflammation caused by mesotherapy, the skin tissues of the mice were stained using Hematoxylin and Eosin (H&E). During the 2nd, 4th, and 8th weeks, the mice were anesthetized with 10% sodium pentobarbital, followed by fur shaving and euthanasia. The collected skin tissues were preserved in 4% paraformaldehyde for 48 hours at room temperature and then embedded in paraffin. The paraffin-embedded tissue sections were subsequently processed for H&E staining.

The potential of mesotherapy to stimulate collagen regeneration was assessed using Masson's trichrome staining on mouse skin tissues. At the 2nd, 4th, and 8th weeks, after anesthesia with sodium pentobarbital, the mice were euthanized. Skin samples were collected, fixed in 4% paraformaldehyde, and embedded in paraffin. The tissue sections were then stained with Masson's trichrome to evaluate collagen deposition.

2.5.5. Effect of Col-M on hydroxyproline, MDA, SOD, and GSH levels

To assess the efficacy of mesotherapy in promoting collagen regeneration, hydroxyproline concentration was measured as previously described. Briefly, 20 mg of skin tissue that had been defatted was minced and incubated in 2 mL of 6 M HCl at 85 ℃ for 12 hours. The pH was adjusted to 7.0 with 10 mol/L NaOH at room temperature. Hydroxyproline standard solutions were prepared at concentrations of 5.0, 7.5, 10, 15, and 20 μg/mL. Chloramine-T was added to the mixture and incubated at room temperature for 20 minutes, followed by the addition of Ehrlich's reagent and incubation at 85 ℃ for 10 minutes. The mixture was then cooled to room temperature and left to incubate for an additional 30 minutes. Absorbance at 560 nm was measured, and hydroxyproline concentrations in the hydrolyzed samples were calculated using the standard curve. Hydroxyproline concentrations in the tissue homogenates were expressed per milligram of dry tissue.

The levels of malondialdehyde (MDA), superoxide dismutase (SOD), and glutathione reductase (GSH) were quantified using colorimetric assay kits. Initially, skin tissues were weighed and immersed in extraction solution at a ratio of 0.1 g/mL, then homogenized on ice. The resulting homogenate was centrifuged at 8000 × g for 10 minutes at 4 ℃, and the supernatant was collected. This supernatant was subsequently analyzed using a microplate reader to measure the concentrations of MDA, SOD, and GSH.

2.6. Statistical analysis

Data are presented as the mean ± standard error of the mean (SEM). Statistical significance was determined using one-way analysis of variance (ANOVA) in SPSS 24.0, followed by least significant difference (LSD) post hoc tests. Graphs were generated in GraphPad Prism. Significance levels were set as follows: *$p < 0.05$, **$p < 0.01$, and ***$p < 0.001$.

3. Results

3.1. Screening of multifunctional Col-M

The antioxidant capacities of the VC + Col, GSH + Col, and Cys + Col composite solutions were assessed through DPPH and ABTS radical scavenging assays (Figure 1). The VC + Col, GSH + Col,

and Cys + Col solutions effectively scavenged free radicals, with their scavenging abilities showing a positive correlation with increasing concentrations. At a concentration of 0.04 mg/mL, the VC + Col solution achieved a DPPH radical scavenging rate of approximately 90%, whereas, at the same concentration, the scavenging rates of the GSH + Col and Cys + Col solutions were below 60% (Figure 1a). When the concentration of the antioxidant components reached 0.06 mg/mL, the VC + Col solution exhibited an ABTS radical scavenging rate approaching 100%. In contrast, the GSH + Col and Cys + Col solutions did not exceed 80% (Figure 1b). These results suggested that the VC + Col composite solution demonstrated the highest radical scavenging ability and antioxidant capacity. Notably, similar DPPH and ABTS scavenging activities have been reported for *Sargassum serratifolium* extracts, which showed strong radical scavenging ability [35].

The whitening efficacy of the An + Col, TC + Col, VB3 + Col, and H-9 + Col composite solutions was evaluated using tyrosinase inhibition assays (Figure 1c). The inhibition rates of tyrosinase increased as the concentrations of An, TC, VB3, and H-9 in the composite solutions rose. At a concentration of 0.1 mg/mL, An + Col displayed an inhibition rate of approximately 50%. In contrast, the inhibition rates of TC + Col, VB3 + Col, and H-9 + Col were all below 50% at this same concentration (Figure 1c). These findings indicated that the An + Col composite solution demonstrated the most significant tyrosinase inhibition effect, implying superior whitening efficacy. This observation aligns with previous findings that fish scale-derived peptides can effectively inhibit tyrosinase activity and suppress melanin formation *in vitro* [36]. This further suggested the potential of Col-M as whitening agents of skin.

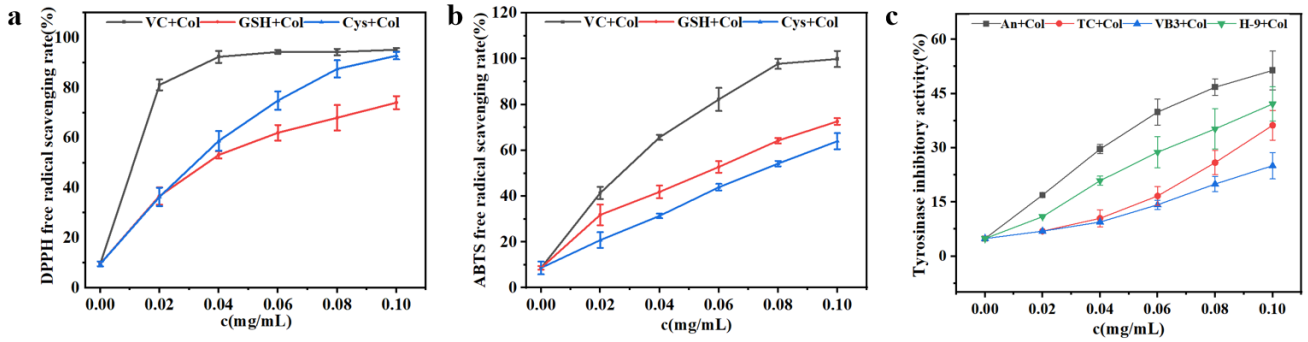

Figure 1. The DPPH **(a)** and ABTS **(b)** free radical scavenging activities of collagen combined with varying concentrations of antioxidant components. The tyrosinase inhibitory ability of collagen combined with different concentrations of whitening components **(c)**.

3.2. Zebrafish efficacy evaluation

To further clarify the efficacy of yak collagen in combination with hydrating, tissue-repairing, anti-wrinkle, and soothing components, a series of experiments utilizing zebrafish was conducted (Figure 2).

The hydrating capabilities of HA + Col, Ceramide + Col, DTd + Col, DG + Col, and Col were assessed using zebrafish hydration experiments (Figure 2a). The model group showed a significant reduction in both tail area and tail length compared to the normal group, confirming the successful establishment of the zebrafish hydration assessment model (Figure 2a). The HA + Col group demonstrated the least variation in both tail length and caudal fin area, with a relative caudal fin area of 87.17% and a relative tail length of 95.80% (***$p < 0.001$) (Figure 2d,e). In contrast, the Ceramide + Col, DTd + Col, DG + Col, and Col groups exhibited lower relative caudal fin areas and lengths

compared to the HA + Col group. The results suggested that HA + Col possesses the most effective hydrating properties.

Zebrafish tissue repair experiments were conducted to evaluate the tissue-repairing capabilities of GHK + Col, Ceramide + Col, BFE + Col, Allantoin + Col, Cae + Col, and Col (Figure 2b). The GHK + Col group revealed the largest caudal fin area, measuring 318,226 pixels, while the caudal fin areas of Ceramide + Col, BFE + Col, Allantoin + Col, Cae + Col, and Col were all smaller (***$p < 0.001$) (Figure 2f). This repair-promoting trend is consistent with previous findings on recombinant type III collagen (rCol III), which significantly enhanced zebrafish caudal fin regeneration [37]. These findings indicated that the GHK + Col composite solution possessed the strongest tissue-repairing capability.

The anti-wrinkle effects of L-Carnosine + Col, PDRN + Col, NMN + Col, β-glucan+Col, BFE + Col, and Col were examined in a zebrafish anti-wrinkle experiment (Figure 2c,i). In the normal group, zebrafish were not exposed to UV radiation and showed smooth and intact caudal fins. Conversely, in the model group, zebrafish displayed rough and wrinkled caudal fins after UV radiation, thereby confirming the successful establishment of the model (Figure 2c). This experiment measured the caudal fin area of the zebrafish embryos following UV-induced wrinkling (Figure 2i). The NMN + Col group achieved an anti-wrinkle rate of 95.00% (***$p < 0.001$). In comparison, the anti-wrinkle rates of the L-Carnosine + Col, PDRN + Col, BFE + Col, and Col groups were all lower than that of the NMN + Col group, indicating that NMN + Col demonstrated the most robust anti-wrinkle capacity. This effect is comparable to that observed with recombinant human elastin (rElastin), which has also been shown to effectively prevent fin architecture deterioration in similar models [38].

The soothing effects of NMN + Col, PDRN + Col, Cae + Col, Allantoin + Col, and Col were evaluated through zebrafish experiments. The PDRN + Col group exhibited the lowest embryonic spin counts, with a stimulation intensity of 190.91% (***$p < 0.001$) (Figure 2g,h). In contrast, the NMN + Col, Cae + Col, Allantoin + Col, and Col groups all showed higher embryonic spin counts and stimulation intensities than the PDRN + Col group. These findings indicate that PDRN + Col offers the most effective soothing effect.

The findings from the circular dichroism (CD) spectra demonstrated that the yak collagen within Col-M maintained its fully intact triple-helix structure (Figure S1). The cytotoxicity of Col-M was assessed using CCK-8 assays (Figure S2), showing that cell viability exceeded 100% across Col-M concentrations ranging from 20% to 200% compared to the blank group. Furthermore, findings related to pyrogenicity and hemocompatibility collectively confirm the remarkable biocompatibility of Col-M (Figure S3(a–c)). This study focused on the short-term safety evaluation of yak collagen mesotherapy, including hemolysis and pyrogen tests. Long-term safety aspects such as immunogenicity and potential allergenicity were not addressed. Future studies are planned to investigate these factors comprehensively to ensure the clinical safety of the product.

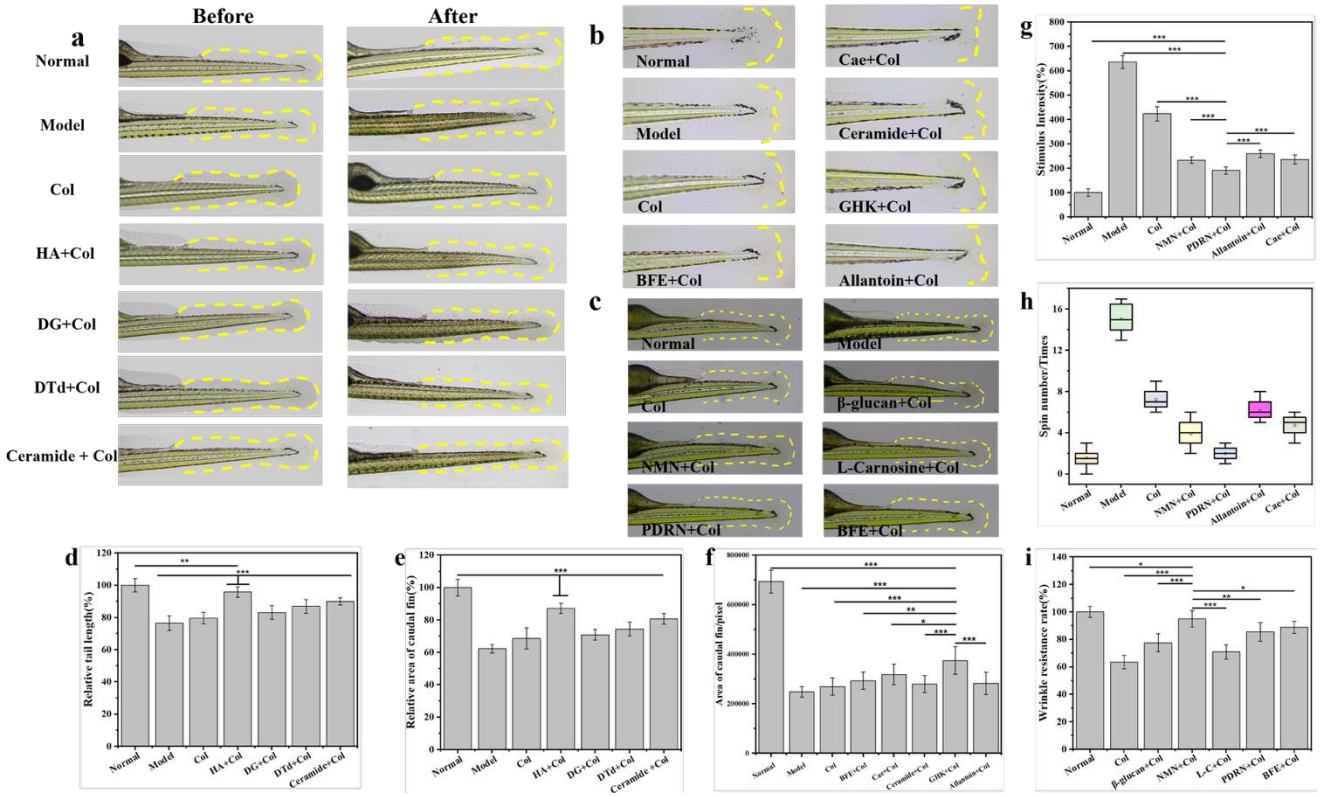

Figure 2. Evaluation of zebrafish efficacy of different functional ingredients combined with yak collagen solution. Phenotypic chart **(a)**, caudal fin area bar chart **(d)**, and tail length bar chart **(e)** of the moisturizing effect of Col combined with moisturizing ingredients on zebrafish. The effects of Col combined with different tissue repair promoting components on zebrafish caudal fin tissue regeneration **(b, f)**. The anti-wrinkle effects of Col combined with different anti-wrinkle ingredients on zebrafish **(c, i)**. The effect of Col combined with different soothing ingredients on the stimulation intensity **(g)** and embryo spin frequency **(h)** of zebrafish stimulation model.

3.3. Performance evaluation of yak collagen mesotherapy with Combo

Photoaging refers to premature aging characterized by the development of wrinkles, fine lines, skin thickening, and dehydration [39,40]. Col-M was injected into photoaged mice, and skin characteristics, including appearance and density, were assessed at weeks 2, 4 and 8. Combo dermatoscopy was employed to evaluate the appearance of mice's skin (Figure 3a). The normal group exhibited no wrinkles; in contrast, the model group displayed prominent wrinkles, while the skin of the Col and control groups showed mild wrinkling. Notably, the Col-M group demonstrated no signs of wrinkles. These findings indicated that Col-M effectively mitigated wrinkle formation.

The restorative ability of Col-M on photoaged mouse skin was evaluated by measuring skin density using combo ultrasound (Figure 3b). The ultrasound signals were categorized by intensity as follows: white > yellow > red > blue > green > black [41,42]. dermal density decreased in both the model and Col groups, whereas the control and Col-M groups showed improvements, nearing levels comparable to normal skin. At week 8, the Col group exhibited an increase in dermal density. However, the Col-M group surpassed normal skin levels. These results suggested that Col-M treatment could accelerate the recovery of photoaged skin, achieving normal thickness and density. The Col group performed slightly

worse than the control group, which may be closely related to the composition of the formulations used. The control group received a commercially available mesotherapy product containing multiple bioactive components, such as vitamins, minerals, coenzymes, and amino acids, whereas the Col group was treated with a single-component collagen solution. The superior therapeutic effect observed in the control group may be attributed to the synergistic actions of its various active ingredients, which collectively promote skin repair, enhance hydration, and improve antioxidant capacity. The differences in formulation composition between the two groups are likely key factors contributing to the observed variation in treatment outcomes.

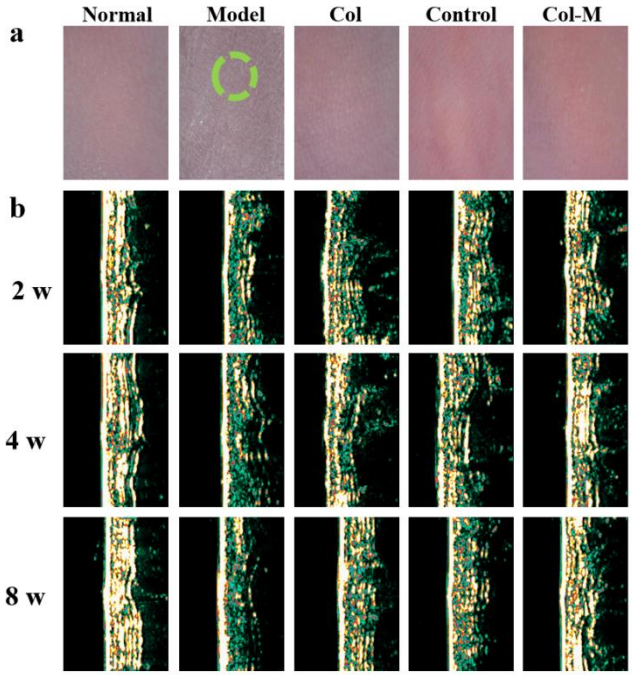

Figure 3. Evaluation of Col-M repair performance using ultrasound and dermatoscopy. Skin microscopy **(a)** and ultrasound skin imaging **(b)** of mice skin in injection of different groups, including Normal, Model, Col, Control and Col-M.

The efficacy of Col-M in repairing photoaged skin was evaluated by measuring density, color, moisture, and TEWL (Figure 4). Dermis density was assessed to determine Col-M's effect on restoring skin density (Figure 4a). Higher values indicated better skin condition. Throughout the experiment, the dermal density of the normal group remained high, while the model group showed a gradual decrease in dermal density due to UV damage, which degraded and depleted collagen. At week 2, the dermal density of the Col, Control, and Col-M groups was close to that of the normal group. At weeks 4 and 8, the dermal density of the Col-M group increased gradually. Notably, from week 4 onwards, the dermal density of the Col and Control groups started to decrease compared to the normal group. These results suggested that the Col-M improved dermal density in photoaged skin.

The effectiveness of Col-M in enhancing skin brightness was quantitatively examined using the Combo melanin probe (Figure 4b). At week 2, melanin levels in the model, Col, Control, and Col-M groups were higher than those in the normal group. By weeks 4 and 8, the skin tone in both the Control and Col-M groups gradually approached that of the normal group, with the Col-M group showing a

lighter skin color compared to the Control group. These results suggested that Col-M contributed to the restoration of skin color in photoaged skin.

The impact of Col-M on skin moisture restoration was quantified using the Combo hydration probe (Figure 4c). At week 2, moisture content in the model and Col groups was lower than that in the normal group, whereas the control group's moisture content was comparable to that of the normal group. The moisture content in the Col-M group was greater than that in the normal group. At weeks 4 and 8, moisture content in the Col and Control groups remained lower than that in the normal group, while the moisture content in the Col-M group was comparable to that of the normal group. These findings suggested that Col-M contributed to the restoration of moisture levels in photoaged skin.

The TEWL value reflected the amount of water lost from the skin due to evaporation through the epidermis [43]. By week 2, the TEWL values in the Col and Control groups showed a slight increase compared to the normal group, while the Col-M group maintained values consistent with those of the normal group. By weeks 4 and 8, the TEWL in the Col and Control groups rose significantly, whereas the Col-M group maintained comparable levels. These results suggested that Col-M effectively repaired the skin barrier in photoaged skin, promoting the restoration of normal TEWL levels. Similar recovery trends were also reported in the Combo system evaluation of agarose hydrogel implants in a photoaging model [44].

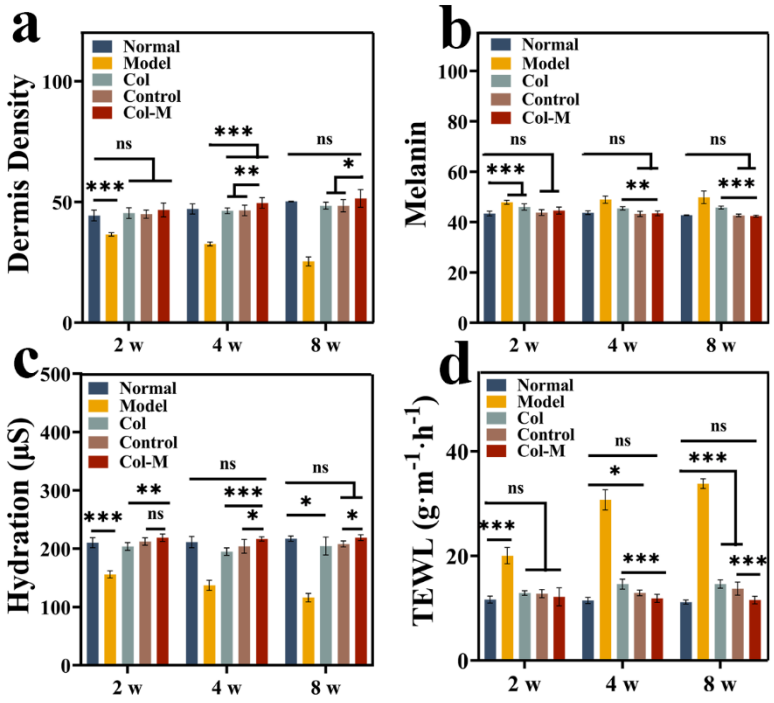

Figure 4. Combo evaluation the performance of Col-M. The skin dermis density **(c)**, melanim **(b)**, hydration **(c)** and TEWL **(d)** of mice skin in injection of different groups, including Normal, Model, Col, Control, and Col-M.

3.4. Histological analysis of the biological activity of Col-M

H&E staining was used to assess the levels of inflammation in the skin tissues of mice injected with Col-M (Figure 5a). At 2, 4 and 8 weeks post-injection, no inflammatory response was observed in the normal

group, whereas the control group exhibited inflammatory cell infiltration. No significant inflammation or granuloma was observed in the Col, control, and Col-M groups. These results indicated that the injection of Col-M did not cause significant inflammatory reactions.

Epidermal thickness measurements were employed to quantitatively assess the impact of Col-M on epidermal thickness (Figure 5b). At week 2, no significant differences were observed between the groups, except for the model group. By week 4, the epidermal thickness of the model and control groups increased significantly, whereas the Col and Col-M groups exhibited thickness levels comparable to the normal group. At week 8, the model and control groups maintained elevated epidermal thickness, while the Col and Col-M groups displayed only a slight increase compared to the normal group. These findings suggested that Col-M aided in the restoration of epidermal thickness in photoaged skin, which is consistent with previous findings that Bouea macrophylla extract (BME) effectively suppressed UV-induced skin thickening, thereby alleviating photoaging [40].

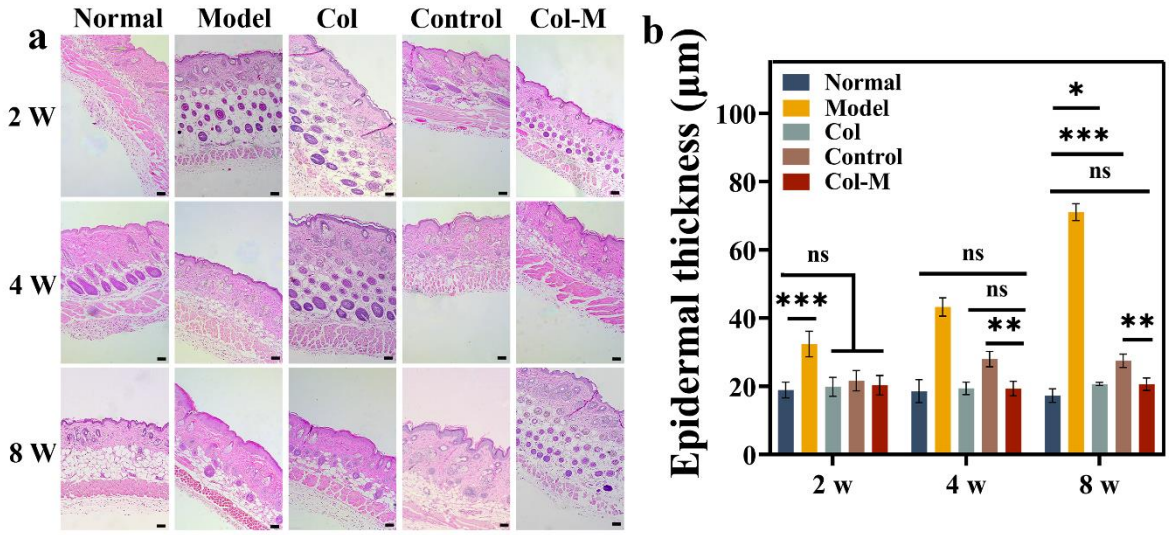

Figure 5. H&E staining of mice skin in injection of different groups, including Normal, Model, Col, Control, and Col-M groups (scale bar:70 μm) **(a)**. Epidermal thickness of mouse skin was quantified using Image J **(b)**.

Masson staining was used to evaluate the capacity of Col-M to repair and regenerate collagen fibers in photoaged skin (Figure 6). Collagen was considered to be a space-filling material in extracellular matrix (ECM) to provide mechanical support and tissue integrity [45]. In the normal group, collagen fibers in the dermal layer maintained a wavy and orderly arrangement throughout the experiment. At week 2, varying degrees of collagen disruption and loosening of the structure were observed in the model, Col, Control, and Col-M groups, with the model group exhibiting the most severe damage. By week 4, the disrupted collagen fibers in the Col, Control, and Col-M groups showed progressive repair and more organized alignment compared to the model group. By week 8, while the model group still displayed pronounced collagen fiber disruption, the dermal collagen fibers in the Col, Control, and Col-M groups appeared denser and better aligned (Figure 6a). The collagen volume fraction obtained from Masson staining analysis via ImageJ showed similar trends in collagen regeneration (Figure 6b). These results suggested that Col-M could improve collagen structure and accelerated the remodeling process in photoaged skin.

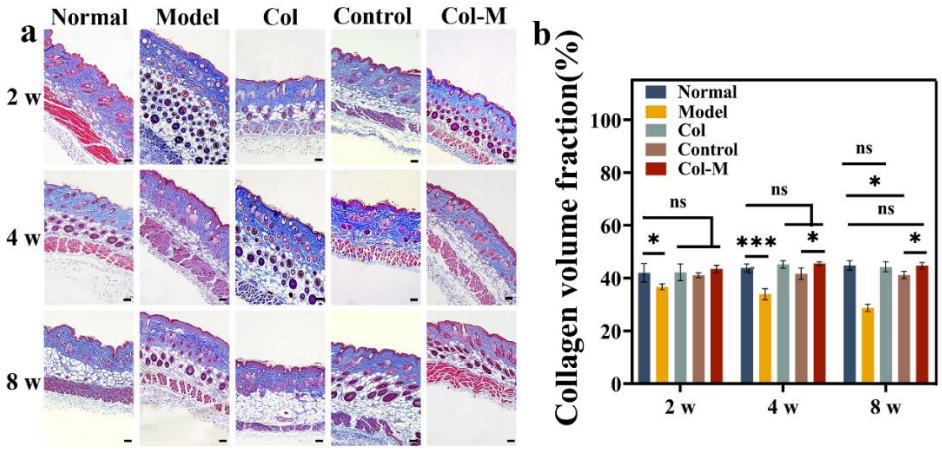

Figure 6. Masson staining evaluation of the ability of Col-M to promote collagen regeneration. Masson staining images (scale bar:70 μm) with yellow arrows indicating the rupture sites of collagen fibers **(a)** and collagen fraction volume **(b)** of the Normal, Model, Col, Control, and Col-M groups at weeks 2, 4 and 8.

The hydroxyproline content was measured to further evaluate the effect of Col-M on collagen regeneration (Figure 7a). After 8 weeks of treatment, the normal group showed a relative hydroxyproline content of 99.92%, while the model group exhibited a significantly lower level of 44.17%. In the Col group, the hydroxyproline content reached 87.26%, and in the Control group, 80.12%. Notably, the Col-M group demonstrated a relative hydroxyproline content of 101.10%, highlighting Col-M's strong potential to promote collagen regeneration. This is consistent with the findings of Wang *et al.*, who reported that agarose microsphere implants restored photoaged skin by promoting collagen regeneration [46].

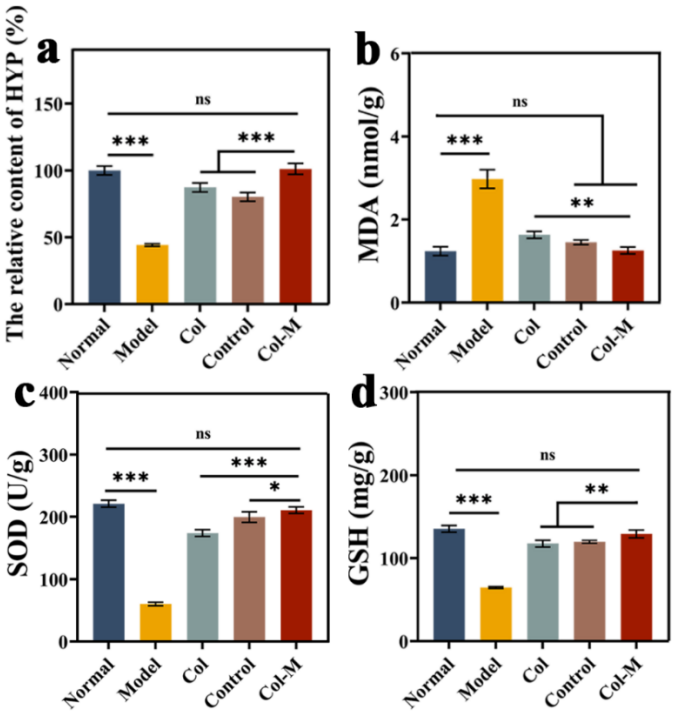

Figure 7. The quantitative analysis of the effect of Col-M on the repair of photoaged skin. The content of Hyp **(a)**, MDA **(b)**, SOD **(c)**, and GSH **(d)** in the Normal, Model, Col, Control, and Col-M groups at week 8.

To assess the reparative effect of Col-M on UV-induced skin aging, SOD activity, MDA content, and GSH levels were measured (Figure 7b–d). Prolonged UV exposure increased reactive oxygen species (ROS), leading to decreased SOD activity and GSH levels, while accelerating lipid peroxidation, resulting in elevated MDA production. The SOD activities in the normal, model, Col, Control, and Col-M groups were 221.14, 60.28, 173.97, 199.65, and 210.81 U/g, respectively. The corresponding MDA levels were 1.24, 2.97, 1.63, 1.45, and 1.25 nmol/g, and GSH contents were 135.33, 64.57, 117.57, 119.76, and 129.19 mg/g, respectively. These results suggested that Col-M increased SOD activity and GSH levels, while simultaneously reducing MDA levels, thereby effectively counteracting UV-induced skin aging. This is in agreement with previous findings that resveratrol isolated from mulberry reduced MDA content and enhanced SOD activity in oxidatively damaged cells, thereby alleviating oxidative stress [47].

4. Conclusion

Photoaging of the skin is a consequence of prolonged exposure to UV radiation, leading to issues such as decreased skin hydration and increased wrinkle formation, which negatively impact patients' daily lives and psychological well-being. The application of hyaluronic acid mesotherapy is restricted due to its short duration of effect and suboptimal efficacy. While recombinant collagen mesotherapy offers benefits such as biocompatibility and biosafety, its high cost and singular efficacy limit its application in skin aesthetics.

In this study, we developed a multifunctional Col-M with high biosafety and bioactivity, exhibiting exceptional collagen regeneration and whitening capabilities for the repair of photoaged skin. Circular dichroism spectra revealed that the yak collagen within Col-M preserved its intact triple-helix structure. The cell experiments demonstrated that the Col-M exhibited excellent cellular activity. Furthermore, the pyrogenicity and hemocompatibility test results consistently demonstrated the excellent biosafety profile of Col-M. We will also systematically conduct long-term safety studies including immunogenicity assessments, allergenicity evaluation, and 12-month chronic toxicity observations.

In photoaged mouse models, Combo dermatoscopy indicated that the Col-M markedly enhanced dermal density and stimulated collagen regeneration. Col-M improved skin tone and moisture levels while mitigating transepidermal water loss. Additionally, Col-M stimulates collagen regeneration without causing an inflammatory response. As a novel mesotherapy, Col-M shows promising applications in the fields of dermatology.

5. Supplementary data

The authors confirm that the supplementary data are available within this article.

Acknowledgments

The authors appreciate the financial support from the National Natural Science Foundation of China (grant no. 22305107, 21775059 and 22074057), the Natural Science Foundation of Gansu Province (grant no. 20YF3FA025 and 18YF1NA004).

Authors' contribution

Shimeng Xu: investigation, data curation, formal analysis, writing-original draft, resources. Yi Yang: data curation, formal analysis. Jingting Zhang: resources. Guangyu Liu: resources. Xiuxia Sun: formal analysis, conceptualization, validation, writing—review & editing, funding acquisition, resources. Jianxi Xiao: conceptualization, project administration, writing—review & editing, funding acquisition, resources.

Conflicts of interests

The authors declare no conflicts of interest.

References

[1] Chaudhary M, Khan A, Gupta M. Skin ageing: pathophysiology and current market treatment approaches. *Curr. Aging Sci.* 2020, 13(1):22–30.

[2] Landau M. Exogenous factors in skin aging. *Environ. Factors in Skin Dis.* 2007, 35:1.

[3] Lombardi F, Augello FR, Ciafarone A, Ciummo V, Altamura S, *et al.* 3D models currently proposed to investigate human skin aging and explore preventive and reparative approaches: a descriptive review. *Biomolecules* 2024, 14(9):1066.

[4] Chen X, Yang C, Jiang G. Research progress on skin photoaging and oxidative stress. *Postepy Dermatol. Alergol.* 2021, 38(6):931–936.

[5] Chung JH, Hanft VN, Kang S. Aging and photoaging. *J. Am. Academy of Dermatol.* 2003, 49(4):690–697.

[6] Vierkötter A, Krutmann J. Environmental influences on skin aging and ethnic-specific manifestations. *Derm.-Endocrinol.* 2012, 4(3):227–231.

[7] Huang AH, Chien AL. Photoaging: a review of current literature. *Curr. Dermatol. Rep.* 2020, 9(1):22–29.

[8] Burla F, Dussi S, Martinez-Torres C, Tauber J, van der Gucht J, *et al.* Connectivity and plasticity determine collagen network fracture. *Proc. Natl. Acad. Sci.* 2020, 117(15):8326–8334.

[9] Cenaj O, Allison DHR, Imam R, Zeck B, Drohan LM, *et al.* Evidence for continuity of interstitial spaces across tissue and organ boundaries in humans. *Commun. Biol.* 2021, 4(1):436.

[10] Lan CCE, Hung YT, Fang AH, Ching-Shuang W. Effects of irradiance on UVA-induced skin aging. *J. Dermatol. Sci.* 2019, 94(1):220–228.

[11] Stoian AP, Hainarosie R, Pietrosanu C, Rusescu A, Andronache LF, *et al.* Modern concepts in non-surgical esthetics; a review. *J. Mind and Med. Sci.* 2019, 6(2):190–195.

[12] Scarano A, Qorri E, Sbarbati A, Desiderio V, Amuso D. Mesotherapy with HA and Choline against facial skin aging: an open-label uncontrolled, monocentric study. *J. Clin. Med. Res.* 2025, 14(7):2303.

[13] Scarano A, Qorri E, Sbarbati A, Gehrke SA, Marchetti M, *et al.* Mesotherapy with hyaluronic acid solutions enriched by amino acids in the neck area: open-label uncontrolled, monocentric study. *J. Costmet Laser Ther.* 2025, 27:121–126.

[14] Duteil L, Queille-Roussel C, Issa H, Sukmansaya N, Murray J, *et al.* The effects of a non-crossed-linked hyaluronic acid gel on the aging signs of the face *versus* normal saline: a randomized, double-blind, placebo-controlled, split-faced study. *J. Clin. Aesthetic Dermatol.* 2023, 16(2):29.

[15] Yi KH, Winayanuwattikun W, Kim SY, Wan J, Vachatimanont V, *et al.* Skin boosters: definitions and varied classifications. *Skin Res. Technol.* 2024, 30(3):e13627.

[16] Arora G, Arora S, Sadoughifar R, Batra N. Biorevitalization of the skin with skin boosters: concepts, variables, and limitations. *J. Cosmetic Dermatol.* 2021, 20(8):2458–2462.

[17] Lee JH, Kim J, Lee YN, Choi S, Lee YI, *et al.* The efficacy of intradermal hyaluronic acid filler as a skin quality booster: a prospective, single center, single arm pilot study. *J. Cosmetic Dermatol.* 2024, 23(2):409–416.

[18] Sadlik J, Kosińska E, Słota D, Niziołek K, Tomala A, *et al.* Bioactive hydrogel based on collagen and hyaluronic acid enriched with freeze-dried sheep placenta for wound healing support. *Int. J. Mol. Sci.* 2024, 25(3):1687.

[19] Wang J, Qiu H, Xu Y, Gao Y, Tan P, *et al.* The biological effect of recombinant humanized collagen on damaged skin induced by UV-photoaging: an *in vivo* study. *Bioact Mater.* 2022, 11:154–165.

[20] Wang T, Lew J, Premkumar J, Poh CL, Win Naing M. Production of recombinant collagen: state of the art and challenges. *Engineering Biology.* 2017, 1(1):18–23.

[21] Wang H. A review of the effects of collagen treatment in clinical studies. *Polymers* 2021, 13(22):3868.

[22] Zhang Y, Wang Y, Li Y, Yang Y, Jin M, *et al.* Application of collagen-based hydrogel in skin wound healing. *Gels* 2023, 9(3):185.

[23] Vrehen AF, van Sprang JF, Schotman MJG, Dankers PY. Collagen type I mimicking peptide additives to functionalize synthetic supramolecular hydrogels. *Materials Today Bio.* 2024, 26:101021.

[24] Fukumoto Y, Tsuji Y, Kakuda A, Hori R, Kudo S. Non-invasive evaluation of autonomic responses in patients with rotator cuff tear-related nocturnal pain. *J. Phys. Ther. Sci.* 2024, 36(3):111–116.

[25] Liu P, Ding L, Zhou Y, Jing X, Degen AA. Behavioural characteristics of yaks grazing summer and winter pastures on the Qinghai-Tibetan Plateau. *Appl. Anim. Behav. Sci.* 2019, 218:104826.

[26] Long RJ, Ding LM, Shang ZH, Guo X. The yak grazing system on the Qinghai-Tibetan Plateau and its status. *Rangeland J.* 2008, 30(2):241–246.

[27] Li F, Jia D, Yao K. Amino acid composition and functional properties of collagen polypeptide from Yak (Bos grunniens) bone. *LWT - Food Sci. Technol.* 2009, 42(5):945–949.

[28] Yang X, Bai Z, Zhang D, Zhang Y, Cui H, *et al.* Enrichment of flavonoid-rich extract from Bidens bipinnata L. by macroporous resin using response surface methodology, UHPLC–Q TOF MS_MS assisted characterization and comprehensive evaluation of its bioactivities by analytical hierarchy process. *Biomed. Chromatogr.* 2020, 34(11):e4933.

[29] Richardson R, Slanchev K, Kraus C, Knyphausen P, Eming S, *et al.* Adult Zebrafish as a model system for cutaneous wound-healing research. *J. Invest. Dermatol.* 2013, 133(6):1655–1665.

[30] Li Q, Frank M, Thisse CI, Thisse BV, Uitto J. Zebrafish: a model system to study heritable skin diseases. *J. Invest. Dermatol.* 2011, 131(3):565–571.

[31] Naomi R, Bahari H, Yazid MD, Embong H, Othman F. Zebrafish as a model system to study the mechanism of cutaneous wound healing and drug discovery: advantages and challenges. *Pharmaceuticals* 2021, 14(10):1058.

[32] Sun L, Gu L, Tan H, Liu P, Gao G, *et al.* Effects of 17α-ethinylestradiol on caudal fin regeneration in zebrafish larvae. *Sci. Total Environ.* 2019, 653:10–22.

[33] Du Y, Li X, Tan D. Comparison of temperature rise interpretations in the rabbit pyrogen test among Chinese, Japanese, European, and United States pharmacopeias and 2-2-2 theoretical models proposed by S. Hoffmann. *Innate Immun.* 2011, 17(5):486–495.

[34] Wang Q, Yan H, Yao L, Xie Y, Liu P, *et al.* A highly bioactive THPC-crosslinked recombinant collagen hydrogel implant for aging skin rejuvenation. *Int. J. Biol. Macromol.* 2024, 266:131276.

[35] Lim S, Choi AH, Kwon M, Joung EJ, Shin T, *et al.* Evaluation of antioxidant activities of various solvent extract from Sargassum serratifolium and its major antioxidant components. *Food Chem.* 2019, 278:178–184.

[36] Ju X, Cheng S, Li H, Xu X, Wang Z, *et al.* Tyrosinase inhibitory effects of the peptides from fish scale with the metal copper ions chelating ability. *Food Chem.* 2022, 390:133146.

[37] Ye M, Fan Y, Fu C, He H, Xiao J. Biocompatible recombinant type III collagen enhancing skin repair and anti-wrinkle effects. *Biomaterials Sci.* 2024, 12(23):6114–6122.

[38] Zhu L, Huang W, Shi J, Li F, Sun X, *et al.* Multipotent anti-aging recombinant human elastin: counteracting zebrafish caudal fin shrinkage and D-galactose-induced intrinsic skin aging in mice. *Int. J. Biol. Macromol.* 2025, 319:145467.

[39] Ain NU, Akhlaq MH, Zhu K, Ji W, Yi L, *et al.* A nanoemulgel formulation of acetylated Crataegus pinnatifida polysaccharide for the treatment of skin photoaging in mice. *Int. J. Biol. Macromol.* 2025, 303:140649.

[40] Cheong Y, Kim C, Kim MB, Hwang JK. The anti-photoaging and moisturizing effects of Bouea macrophylla extract in UVB-irradiated hairless mice. *Food Sci. Biotechnol.* 2018, 27(1):147–157.

[41] De Rigal J, Escoffier C, Querleux B, Faivre B, Agache P, *et al.* Assessment of aging of the human skin by *in vivo* ultrasonic imaging. Leveque. *J. Invest. Dermatol.* 1989, 93(5):621–625.

[42] Lee KC, Dretzke J, Grover L, Logan A, Moiemen N. A systematic review of objective burn scar measurements. *Burns Trauma* 2016, 4(1):14.

[43] Hwang IS, Kim JE, Choi SI, Lee HR, JU LEE Y, *et al.* UV radiation-induced skin aging in hairless mice is effectively prevented by oral intake of sea buckthorn (Hippophae rhamnoides L.) fruit blend for 6 weeks through MMP suppression and increase of SOD activity. *Int. J. Mol. Med.* 2012, 30:392–400.

[44] Guo Y, Tian B, Xie Y, Sun X, Xiao J. Green agarose hydrogel implants with high biocompatibility for skin repair and regeneration in photoaged skin. *Biopolymers* 2025, 116(4):e70032.

[45] Wang J, Hu H, Wang J, Qiu H, Gao Y, *et al.* Characterization of recombinant humanized collagen type III and its influence on cell behavior and phenotype. *J. Leather Sci. Eng.* 2022, 4(1):33.

[46] Wang Q, Yan H, Guo Y, Tian B, Xiao J. High-temperature emulsification coupled with low-temperature gelation for fabrication of agarose microsphere implants with well-controlled size for skin tissue enhancement. *J. Mater. Chem. B* 2024, 12(42):10983–10993.

[47] Zhang L, Chen Q, Chen Z, He T, Yu M, *et al.* Anti-skin aging effects of mulberry fruit extracts: *in vitro* and *in vivo* evaluations of the anti-glycation and antioxidant activities. *J. Funct. Foods* 2024, 112:105984.